Solution structure of a defensin-like peptide from platypus venom

Allan M. TORRES*, Xiuhong WANG*, Jamie I. FLETCHER*, Dianne ALEWOOD†, Paul F. ALEWOOD†, Ross SMITH‡, Richard J. SIMPSON§, Graham M. NICHOLSON‖, Struan K. SUTHERLAND¶, Cliff H. GALLAGHER**, Glenn F. KING* and Philip W. KUCHEL*[1]

*Department of Biochemistry, University of Sydney, NSW 2006, Australia, †Centre for Drug Design and Development, University of Queensland, QLD 4072, Australia, ‡Department of Biochemistry, University of Queensland, QLD 4067, Australia, §Joint Protein Structure Laboratory, Ludwig Institute for Cancer Research and the Walter and Eliza Hall Institute of Medical Research, Parkville, Victoria 3050, Australia, ‖Department of Health Sciences, University of Technology, Sydney, NSW 2007, Australia, ¶The Australian Venom Research Unit, University of Melbourne, Parkville, Victoria 3052, Australia, and **Taronga Zoo, Mosman, NSW 2088, Australia

Three defensin-like peptides (DLPs) were isolated from platypus venom and sequenced. One of these peptides, DLP-1, was synthesized chemically and its three-dimensional structure was determined using NMR spectroscopy. The main structural elements of this 42-residue peptide were an anti-parallel β-sheet comprising residues 15–18 and 37–40 and a small 3_{10} helix spanning residues 10–12. The overall three-dimensional fold is similar to that of β-defensin-12, and similar to the sodium-channel neurotoxin ShI (*Stichodactyla helianthus* neurotoxin I). However, the side chains known to be functionally important in β-defensin-12 and ShI are not conserved in DLP-1, suggesting that it has a different biological function. Consistent with this contention, we showed that DLP-1 possesses no anti-microbial properties and has no observable activity on rat dorsal-root-ganglion sodium-channel currents.

Key words: β-defensin fold, HPLC separation of venom components, NMR of proteins, platypus toxins, protein folding.

INTRODUCTION

The platypus, *Ornithorhynchus anatinus*, is a unique animal that inhabits the fresh water streams and rivers of eastern Australia [1–3]. Although regarded as a mammal, the platypus has many reptilian characteristics. It has fur and mammary glands and yet it lays eggs and has a urogenital system similar to that of reptiles [3,4]. Like other mammals, the platypus is able to regulate its own body temperature; however, its average body temperature is only 32 °C, which is low for a mammal but rather high for a reptile [4].

One peculiar characteristic of the platypus is that the male has a venomous spur located on each hind leg. Of all mammals, only the echidna has a similar venom apparatus [1,3]. It is believed that these toxic spurs are used by the platypus as an offensive weapon against other males to assert dominance during the mating season and perhaps to establish a territory [5]. This hypothesis is supported by the observation that venom production increases during the breeding season, which begins in Spring [1].

At present, knowledge of the nature of platypus venom is limited [1,3,6]. Platypus venom is fatal to dogs but not to humans [1,5,6]. Human envenomation produces an intensely localized pain followed by swelling [7]. There is no available anti-venom [3,7] and general first-aid procedures are ineffective in relieving the pain. The only effective treatment is localized anaesthetic blockade supplemented by narcotic intravenous infusion [7].

In the earliest pharmacological study of the venom, Martin and Tidswell [8] found that subcutaneous injection of venom-gland extract into experimental animals produced local haemorrhage and oedema, while intravenous injection caused hypotension and even death. The similarity of the physiological responses to those elicited by snake venoms was emphasized in this study, although the virulent activity of the platypus venom was considerably weaker than that of common snake venoms. In agreement with this observation, Kellaway and LeMessurier [9] showed that platypus venom possesses weak coagulant, haemolytic and cytolytic activities, similar to those observed in viperine venom. They also found that the venom caused contraction of guinea-pig uterus and jejunum.

Recently, De Plater and co-workers [10,11] renewed the study of the activity and composition of platypus venom. Their investigation confirmed the venom's oedemic activity and found that it relaxes the rat uterus, contrary to the findings of Kellaway and LeMessurier on guinea pigs [9]. Four major protein components, with molecular masses of 4.2, 16, 55 and 140 kDa, were discovered. The 4.2-kDa peptide, which shares a high degree of sequence identity with human and porcine C-type natriuretic peptide, has relaxant, oedema-producing and mast-cell-degranulating activities [11]. NMR studies of similar natriuretic peptides from various mammals revealed their tertiary structures to be flexible with little indication of well-defined secondary structure [12–14]. The other three protein components discovered in platypus venom do not resemble any of the proteins listed in the SwissProt database.

We began a systematic pharmacological and structural characterization of the various components of platypus venom. At present, the focus of attention is on a group of similar peptides of about 5 kDa that are present in significant amounts in the venom. Besides the 4.2-kDa C-type natriuretic peptide identified by De Plater and co-workers [10], peptides in this particular group are the only ones of this size found, so far, in the venom. These peptides were chosen for investigation since their molecular masses are similar to those of known neurotoxins and their three-dimensional structures could be studied readily by NMR spectroscopy. As will be shown later, the amino acid sequences of these peptides have similarities with β-defensin-12, an anti-microbial peptide originally discovered in bovine neutrophils [15]; thus we refer to these peptides as defensin-like peptides (DLPs).

Abbreviations used: DLP, defensin-like peptide; DQF, double-quantum-filtered; TOCSY, total correlation spectroscopy, NOE, nuclear Overhauser enhancement; NOESY, nuclear Overhauser enhancement spectroscopy; RMSD, root-mean-square deviation; RP-HPLC, reverse-phase HPLC; TFA, trifluoroacetic acid; AP-A, anthopleurin-A; ATX, *Anemonia sulcata* toxin; ShI, *Stichodactyla helianthus* neurotoxin I.

[1] To whom correspondence should be addressed (e-mail p.kuchel@biochem.usyd.edu.au).

In this paper, we report the tertiary structure of one of the defensin-like peptides, DLP-1, as determined using NMR spectroscopy and compare this with the structures of β-defensin-12 and other peptides of similar structural folding. It is hoped that the three-dimensional structure will provide clues as to the biological function of DLP-1. We also report here some preliminary activity studies based on the structural similarity between DLP-1 and other peptides.

MATERIALS AND METHODS

Separation and identification of protein components

Fractionation of venom components was performed using reverse-phase HPLC (RP-HPLC) on a GBC HPLC system with LC 1110 pumps controlled by a DP 800 work station. A Vydac C_{18} analytical column was employed in the separation and the solvent system consisted of 0.1 % (v/v) aq. trifluoroacetic acid (TFA) in water (buffer A) and 0.1 % (v/v) aq. TFA in acetonitrile (buffer B). Components were eluted using a flow rate of 1 ml·min^{-1} and linear gradients of 5–20 % buffer B over 5 min followed by 20–45 % buffer B over 40 min. Absorbance was monitored at a wavelength of 215 nm and the eluant was collected manually into polypropylene tubes prior to lyophilization. Molecular masses of the various components were determined using either SDS/PAGE or electrospray MS. Purified components were sequenced by Edman degradation on an Applied Biosystems 473 protein sequencer.

Synthesis, folding and purification

The chain assembly of DLP-1 was performed on a modified ABI 430A synthesizer using t-butoxycarbonyl-chemistry protocols developed in-house [16,17]. Each residue was routinely double-coupled. Prior to HF cleavage, both the DNP and N_{α}-t-butoxycarbonyl protecting groups were removed. Cleavage was effected using HF:*p*-cresol:*p*-thiocresol (18:1:1) at $\sim$0 °C for 1.5 h Crude reduced peptide was purified by elution on a Vydac C_{18} preparative column (2 × 25 cm) using buffer A and a linear gradient from 0 to 25 % buffer C (where buffer C is 90 % acetonitrile/0.085 % aq. TFA) at 1 %·min^{-1}, then from 25 to 40 % C at 0.5 %·min^{-1} at a flow rate of 8 ml·min^{-1} with UV monitoring at 230 nm. The purified peptide (50 mM) was oxidized at 4 °C for 24 h in 0.33 M ammonium acetate buffer, pH 7.8, containing 0.5 M guanidine hydrochloride and glutathione/glutathiol (10:100). The oxidation mixture was purified by RP-HPLC using a linear gradient from 0 to 67 % buffer C at 8 ml·min^{-1} with UV monitoring at 230 nm. Mass-spectral analysis and co-elution with native peptide confirmed that the native and the synthetic material were identical.

Vas deferens assay

Experiments were carried out on isolated rat vas deferens and were set up as follows: first, the isolated tissues were cleaned and desheathed; portions of the bladder end of the tissues, 3-cm long, were then mounted in a 3-ml organ bath containing the bathing fluid consisting of 112.9 mM NaCl, 4.69 mM KCl, 2.52 mM $CaCl_2$, 1.5 mM $MgSO_4$, 1.18 mM KH_2PO_4, 25.0 mM $NaHCO_3$ and 11.0 mM glucose. The organ bath was maintained at 37 °C and equilibrated with 95 % O_2/5 % CO_2.

Tissue contractions were produced by electrical-field stimulation of the vas deferens with three pulses of 20 V every 30 s at a frequency of 10 Hz. The contractions were monitored continuously with an isometric-strain gauge, and were plotted on a chart recorder. Electrical stimulation, when required, was delivered through two parallel, vertical, built-in platinum electrodes in the organ bath. Native venom samples were introduced to the organ bath when the contractions were stabilized after 30–60 min.

Anti-microbial assay

Escherichia coli (XL1-Blue) and *Bacillus subtilis* (wild-type 168) were used in a radial diffusion assay in order to investigate whether DLP-1 had any defensin-like anti-bacterial activity. Bacteria were plated out from cell stocks on to 1.5 % Luria–Bertani agar (*E. coli*) or TBAB (tryptose-blood-agar base) medium (Difco) enriched with 20 μg·ml^{-1} thiamine (*B. subtilis*). Filter-paper discs (6-mm diameter) were spaced evenly on each plate and 10 μl of either DLP-1 (260 μg·ml^{-1}), whole venom or water were pipetted on to the discs. Plates were incubated overnight at 37 °C, then examined for clear zones around each disc.

Electrophysiological recordings

Whole-cell patch-clamp recordings of sodium currents were made from acutely-dissociated dorsal-root-ganglion neurons prepared from 6-day-old Wistar rats according to the methods of Nicholson and co-workers [18]; for these experiments the synthetic peptide was used. Sodium currents were recorded using an Axopatch 200 patch-clamp amplifier (Axon Instruments, Foster City, CA, U.S.A.). Micropipettes (0.67–2 MΩ) were pulled from borosilicate glass capillary tubing and were filled with 135 mM CsF/10 mM NaCl/5 mM Hepes, with pH adjusted to 7.0 with 1 M CsOH. The external solution contained 30 mM NaCl, 1 mM $MgCl_2$, 1.8 mM $CaCl_2$, 5 mM CsCl, 5 mM KCl, 25 mM D-glucose, 5 mM HEPES, 20 mM tetraethylammonium chloride and 70 mM tetramethylammonium chloride, with pH adjusted to 7.4 with 1 M tetraethylammonium hydroxide. Membrane-current recordings were made at ambient temperature (22–25 °C), which did not fluctuate more than 1 °C during the course of an experiment. Large round light dorsal-root-ganglion cells with diameters of 30–35 μm were selected for experiments. In those experiments that assessed the actions of DLP-1 on tetrodotoxin-resistant sodium currents, 200 nM tetrodotoxin was applied in the external solution to eliminate any residual tetrodotoxin-sensitive sodium currents. Stimulation and recording were both controlled by a pClamp data-acquisition system (Axon Instruments). Data were filtered at 5 kHz (low-pass Bessel filter) and the digital sampling rate was 25–50 kHz. Leakage and capacitive currents were subtracted digitally with *P-P/4* procedures and series resistance compensation was > 80 % for all cells.

NMR spectroscopy

An NMR sample was prepared by dissolving 5.1 mg of DLP-1 in 300 μl of 90 % H_2O/10 % ^2H_2O (v/v) in a 5-mm-outer-diameter susceptibilty-matched microcell (Shigemi, Tokyo, Japan) and adjusting the pH to either 2.8 or 3.9. For hydrogen–deuterium-exchange experiments, the sample was lyophilized and reconstituted in 280 μl of 99.96 % ^2H_2O.

The NMR experiments were performed on a Bruker AMX-600 spectrometer operating at either 10 or 25 °C using a 5-mm ^{1}H inverse probe. All two-dimensional homonuclear NMR spectra were acquired in phase-sensitive mode using time-proportional phase detection [19]. The following two-dimensional spectra were recorded: double-quantum-filtered (DQF) scalar correlated spectroscopy [20] with phase cycle modified for fast recycle times [21], total correlation spectroscopy (TOCSY) [22] with MLEV

spin-lock periods of 30, 60 and 90 ms; and nuclear Overhauser enhancement spectroscopy (NOESY) [23] with mixing times of 200 and 300 ms. Water suppression in DQF and NOESY experiments was achieved by low-power irradiation at the water resonance frequency during the relaxation delay in the transients (1.3–1.5 s) and during the mixing period in NOESY experiments. Solvent suppression in the TOCSY experiments was accomplished by using the WATERGATE gradient module [24].

Spectra were processed using XWIN-NMR software (Bruker). Distance constraints were derived from NOESY spectra recorded at pH 3.9 (25 °C) in H_2O and ^2H_2O, with a mixing time of 300 ms. Hydrogen–deuterium-exchange experiments were carried out by reconstituting the lyophilized sample with ^2H_2O, acquiring a series of one-dimensional experiments for 1 h and then acquiring five consecutive 3-h TOCSY experiments. Slowly exchanging amides were interpreted as being hydrogen-bond donors.

Structure calculations

NOESY spectra, analysed using the XEASY program [25], yielded 786 non-redundant interproton distant constraints that were automatically assigned upper-distance limits based on the corresponding cross-peak intensities or volumes. These distance limits were examined thoroughly for errors resulting from peak overlap. A correction of 0.5 Å was added to all upper-distance bounds to allow for conformational averaging and errors in volume integration.

The ϕ dihedral angle constraints were derived from $^3J_{NH\alpha}$ coupling constants either directly measured from one-dimensional NMR spectra or by the inverse Fourier transform of in-phase multiplets from two-dimensional NOESY spectra using the program INFIT [26]. The ϕ angle was constrained to $-60\pm30°$ for $^3J_{NH\alpha} < 5$ Hz; $-60\pm40°$ for $^3J_{NH\alpha} = 5$–6 Hz; $-120\pm30°$ for $^3J_{NH\alpha} = 8$–9 Hz; and $-120\pm20°$ for $^3J_{NH\alpha} > 9$ Hz. The intense HN-Hα nuclear Overhauser enhancement (NOE) cross-peak for Asn-13 and $^3J_{NH\alpha}$ value of ~ 7 Hz permitted its ϕ angle to be constrained to $60\pm20°$ [27]. Hydrogen-bond constraints were deduced from hydrogen–deuterium-exchange experiments and the preliminarily calculated structures; these were introduced only in the final stages of the structure calculations and were constrained with the upper distance limits of 2.2 Å for NH_i to O_j and 3.2 Å for N_i to O_j. Disulphide linkages were obtained from preliminary structures by measuring distances between sulphur atoms and checking the orientation of the cysteine side chains.

The torsion-angle dynamics program DYANA [28] was used in all stages of the structure calculations prior to refinement. In the final structure calculations, 1000 DYANA structures were generated from random starting conformations. The 'best' 50 structures, with the lowest NOE violations, were then refined by simulated annealing in X-PLOR [29]. The simplified all-hydrogen force field was used and the covalent geometry was constrained using the standard X-PLOR parameters. Interatomic distances and dihedral angles were constrained by experimental energy terms ($k_{noe} = 50$ kcal·mol^{-1}·Å^{-2}, $k_{cdihed} = 200$ kcal·mol^{-1}·rad^{-2}), which remained constant throughout the calculations. Initial atomic velocities were set from the Maxwellian distribution at 1000 K, in which all non-bonded interactions are basically ignored, allowing the atoms to pass through each other (repel = 0.9, $C_{rep} = 0.005$ kcal·mol^{-1}·Å^{-2}). Simulated annealing was then performed by gradually 'cooling' the system to 100 K over 20 ps, during which C_{rep} was increased linearly to 4 kcal·mol^{-1}·Å^{-2} while 'repel' was decreased to 0.75. Restrained gradient minimization of 40 cycles was performed in the final stage of the protocol.

The co-ordinates for the ensemble of 20 structures have been deposited with the Brookhaven Protein Data Bank with accession code 1b8w.

RESULTS AND DISCUSSION

Separation, sequence analysis, and synthesis

The various components of the platypus venom were separated using RP-HPLC and were analysed using either SDS/PAGE or MS. Figure 1 shows the RP-HPLC trace of a diluted venom sample with selected peaks labelled. The venom is clearly complex, with at least 10 potentially separable peptide/protein components evident in the RP-HPLC trace. Peaks 1, 2 and 6 were of similar mass, and amino acid sequence analysis revealed that they were similar, as shown in Figure 2. A sequence search performed on the Swiss-Prot database showed that these peptides have no close match with any of the peptides and proteins in the database, but the search did reveal some similarity with β-defensin-12 (see Figure 2).

β-Defensins are a class of 13 similar peptides, isolated from bovine neutrophils, which possess anti-microbial activity against *E. coli* and *Staphylococcus aureus* [15]. These peptides are 38–42 amino acid residues in length, highly cationic and incorporate six conserved cysteine residues. As the molecular masses of the peptides from peaks 1, 2 and 6 were also seen to be similar to β-defensin-12, we chose to refer to this group of molecules as DLPs. DLP-1 and DLP-2 incorporate three disulphide linkages and contain numerous positively charged residues, in a manner analogous to β-defensin-12. On the other hand, DLP-3 has only two disulphide bridges but its sequence is very similar to DLP-2.

Chain assembly of the peptide proceeded smoothly, with the exception of Arg-17 (98.3 %) and Ile-27 (98.8 %, acetylated). The HF cleavage yield was excellent (~ 90 % of theoretical) and the crude reduced peptide was of high purity, with the exception of small amounts of an arginine deletion and a dehydration product. Oxidation of the pure reduced peptide resulted in a single major product, which was isolated in 8 % overall yield. This product was characterized by mass analysis (observed molecular mass 4953.0 ± 0.5 Da; calculated 4953.7 Da) and by co-elution with the native peptide, DLP-1, on a linear gradient (0–67 % buffer B) at 1 %·min^{-1} (results not shown).

NMR peak assignment

NMR peak assignments of DLP-1 were made using standard procedures [30]. No major obstacle was encountered in the assignment process since most of the amide-proton signals of DLP-1 were reasonably intense and narrow, except those of Glu-26, Phe-28 and Arg-41, which were quite broad. Problems of resonance overlap in the amide region were overcome by varying the pH and temperature at which the spectra were acquired.

Structure calculations

Initial structure calculations were performed with DYANA [28] using approx. 600 unambiguous NOE constraints. Whereas the preliminary structures obtained showed a reasonably well-defined three-dimensional fold, the cysteine linkages could not be determined unambiguously. Thorough examination of the NOESY spectra, and inclusion of more NOE constraints, led to better-

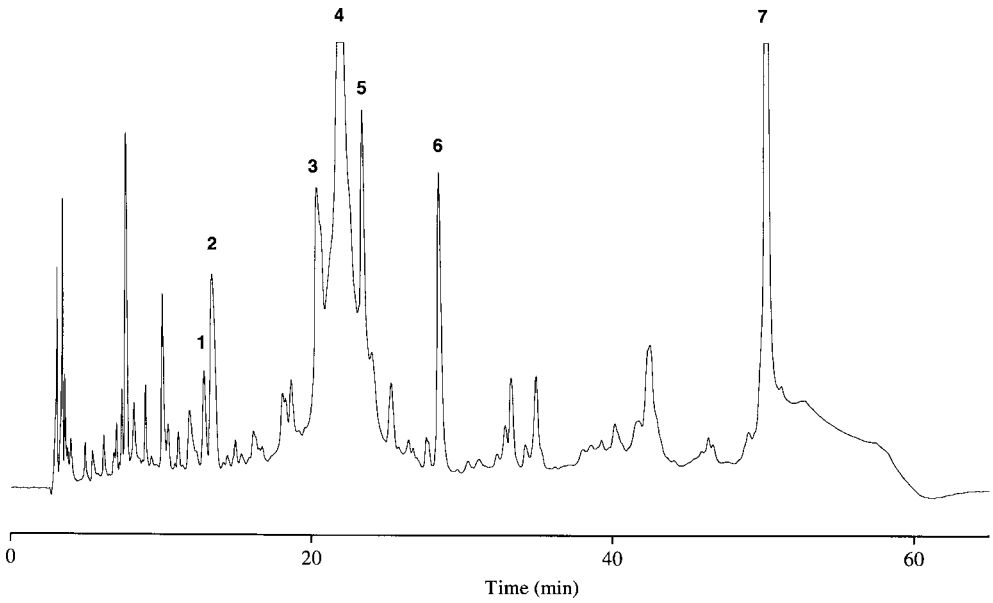

Figure 1 RP-HPLC chromatogram of complete platypus venom

Peaks of components that eluted before component (1) were due to non-proteinaceous species. Labelled peaks correspond to (1) DLP-3, (2) DLP-1, (3) 4.2-kDa C-type natriuretic peptide, (4) 15.1-kDa protein, (5) 5.1-kDa peptide, (6) DLP-2 and (7) 50-kDa protein.

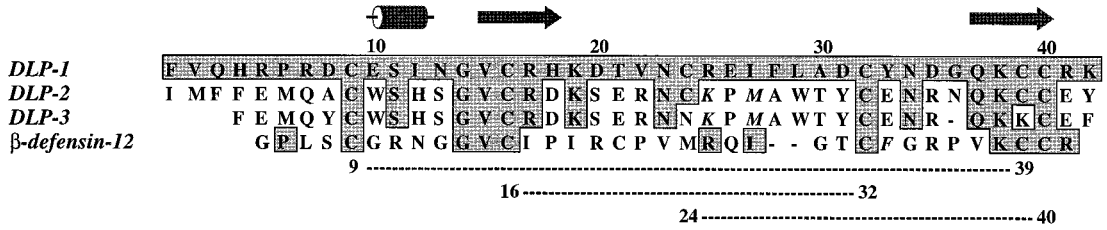

Figure 2 Primary structures of DLPs and β-defensin-12

The amino acid sequences are aligned to show maximum correspondence between them. Similarities are shown relative to DLP-1; identical residues are boxed and conservative substitutions are italicized. The disulphide-bonding pattern determined for DLP-1 from the NMR data is shown below the numbered sequences (dotted lines). The secondary structure of DLP-1 as determined in the current study is shown above the sequences (3_{10} helix is denoted as a cylinder and β-strands are denoted as arrows). The diagram was drawn using ALSCRIPT [44].

defined cysteine side-chain orientations so that the disulphide-pairing patterns of Cys-9–Cys-39, Cys-16–Cys-32 and Cys-24–Cys-40 were deduced. Important NOE interactions between cysteine residues that aided in the identification of the disulphide-bonding pairs included: Cys-9 Hβ–Cys-39 HN; Cys-9 Hβ–Cys-39 Hβ; Cys-16 Hα–Cys-32 Hβ; and Cys-16 Hβ–Cys-32 Hβ. Although NOE cross-peaks Cys-9–Cys-32 and Cys-16–Cys-40 were also found, the former sets of NOE helped considerably in orientating the cysteine side chains so that the Cys-9–Cys-39 and Cys-16–Cys-32 disulphide bonds could be assigned unambiguously. Direct NOE cross-peaks between Cys-24 and Cys-40 could not be assigned unambiguously due to peak overlap; however, the presence of Cys-40 Hβ–Arg-25 HN and Cys-40 Hβ–Glu-26 Hα NOE cross-peaks indicated that the Cys-40 side chain was directed towards Cys-24; in any case, the Cys-24–Cys-40 linkage could be deduced by elimination once the Cys-9–Cys-39 and Cys-16–Cys-32 linkages were assigned.

NOE cross-peaks that could not be unambiguously assigned, *a priori*, were later resolved using a set of low-resolution calculated structures. Slowly exchanging amide protons identified in the ^2H_2O-exchange experiment were helpful in verifying the locations of secondary structural elements that were already identified in medium-resolution structures. Hydrogen-bonding pairs were only deduced from the structure after inclusion of the majority of NOE constraints. The identified hydrogen-bond pairs, together with the cysteine linkages, were only used as constraints during the later stages of the calculation.

Final DLP-1 structures were calculated using a total of 786 non-redundant inter-proton distance constraints, 24 dihedral-angle constraints and 18 hydrogen-bond constraints, giving a total of 828 constraints or 19.7 constraints per residue. The NOE distance constraints consisted of 248 intraresidual, 207 sequential, 146 medium-range and 185 long-range interactions. Structure calculations were performed initially using the simulated annealing protocol in DYANA [28] and then refined by simulated annealing in X-PLOR [29]. Of the 1000 structures generated in DYANA, only the 'best' 50 structures were refined using X-PLOR. The 'best' 20 X-PLOR structures were considered to be representative of the solution structure of DLP-1 and these were used for illustration and statistical analysis.

Table 1 Structural statistics for the ensemble of 20 DLP-1 structures

RMSD, root-mean-square deviation. Values given as means ± S.D.

Distance restraints		
Intraresidue ($i-j=0$)	248	
Sequential ($\|i-j\|=1$)	207	
Medium range ($\|i-j\|\leqslant 5$)	146	
Long range ($\|i-j\|$ 5)	185	
Hydrogen bonds	18	
Total	804	
Dihedral-angle restraints		
ϕ	24	
Mean RMSD from experimental restraints		
NOE (Å)	0.0144 ± 0.0003	
Dihedrals (°)	0.36 ± 0.07	
Mean RMSD from idealised covalent geometry*		
Bonds (Å)	0.00160 ± 0.00004	
Angles (°)	0.326 ± 0.002	
Impropers (°)	0.133 ± 0.008	
Mean energies (kJ · mol^{-1})		
E_{NOE}†	8.21 ± 0.34	
E_{cdih}†	0.19 ± 0.07	
E_{vdW}	0.40 ± 0.06	
E_{bond}	1.73 ± 0.09	
$E_{improper}$	0.98 ± 0.12	
E_{angle}	19.64 ± 0.31	
E_{total}	31.14 ± 0.47	
Atomic RMS differences (Å)‡	Versus mean	Pairwise
Backbone atoms (7–42)	0.29 ± 0.04	0.40 ± 0.09
Heavy atoms (7–42)	0.78 ± 0.08	1.09 ± 0.16

* Idealised geometry as defined by the CHARMM force field within X-PLOR.

† Final values of the square-well NOE and dihedral-angle potentials calculated with force constants of 50 kcal · mol^{-1} · Å^{-2} and 200 kcal · mol^{-1} · Å^{-2}, respectively.

‡ Atomic differences given as average RMS difference against mean co-ordinate structure (mean) and average RMS difference of all pairwise structures (pairwise).

A summary of the structural statistics for this ensemble of structures is provided in Table 1. The ensemble of 20 DLP-1 structures was found to have good covalent geometry, as indicated by low deviations from idealized geometry and good non-bonded contacts, as evidenced by the low mean value of the Lennard-Jones potential (vdW). None of these structures had NOE violations greater than 0.2 Å or dihedral-angle violations greater than 2 °.

Structural analysis

Well-defined regions in the ensemble of structures are indicated by the backbone angular-order parameters for ϕ and ψ angles [31] and the root-mean-square differences (RMSD) from the mean structure. Analysis of the backbone angular parameter (S) of the 20 best structures revealed that residues 1–4, 6, 7, 28, 29, 34 and 35 were less well defined than the rest with $S < 0.800$ for one or both ϕ and ψ angles. This was basically in accordance with the global backbone RMSD with respect to the mean structure, which was $\leqslant 1.0$ Å for all residues except 1–6. The mean global backbone RMSD with respect to the mean structure was 1.17 ± 0.42 Å; this decreased dramatically to 0.29 ± 0.04 Å when only the well-defined region (7–42) was considered.

Figure 3 shows the ensemble of 20 structures superimposed over the backbone of the well-defined region (residues 7–42). It is clear that the N-terminal region, comprising residues 1–6, is less well defined than the rest of the molecule, implying that this part of the molecule is more flexible. Closer examination of the ensemble of structures showed that certain parts of the well-defined region are better defined than others. Specifically, residues 10–20 and 36–40, which constitute defined secondary structural elements, such as 3_{10} helix and β-strands, had lower RMSDs than other regions.

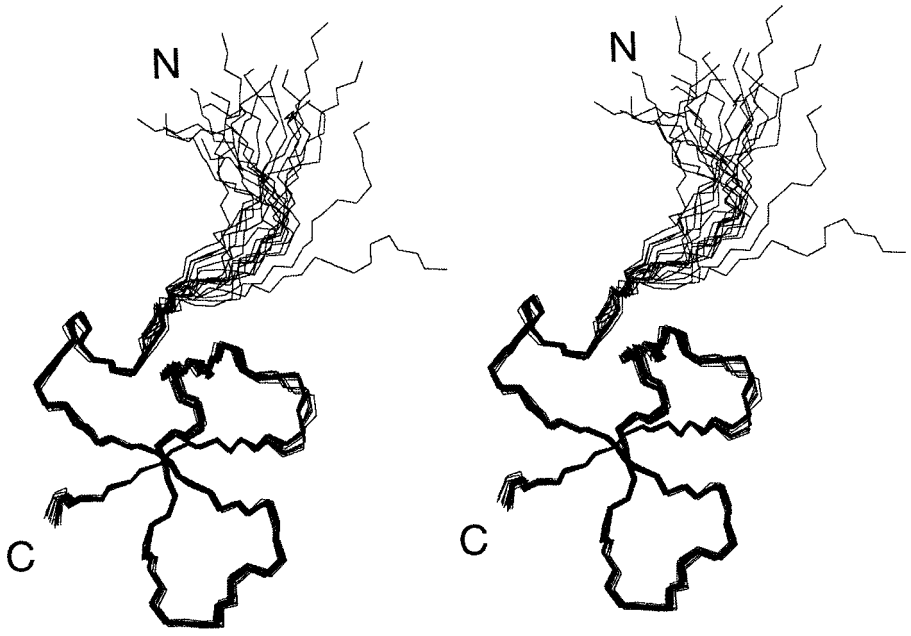

Figure 3 Ensemble of 20 DLP-1 structures

Stereo view of the ensemble of 20 DLP-1 structures superimposed to show the best fit over the backbone atoms of residues 7–42 of the mean co-ordinate structure. Only the N, C and Cα atoms of the backbone are displayed.

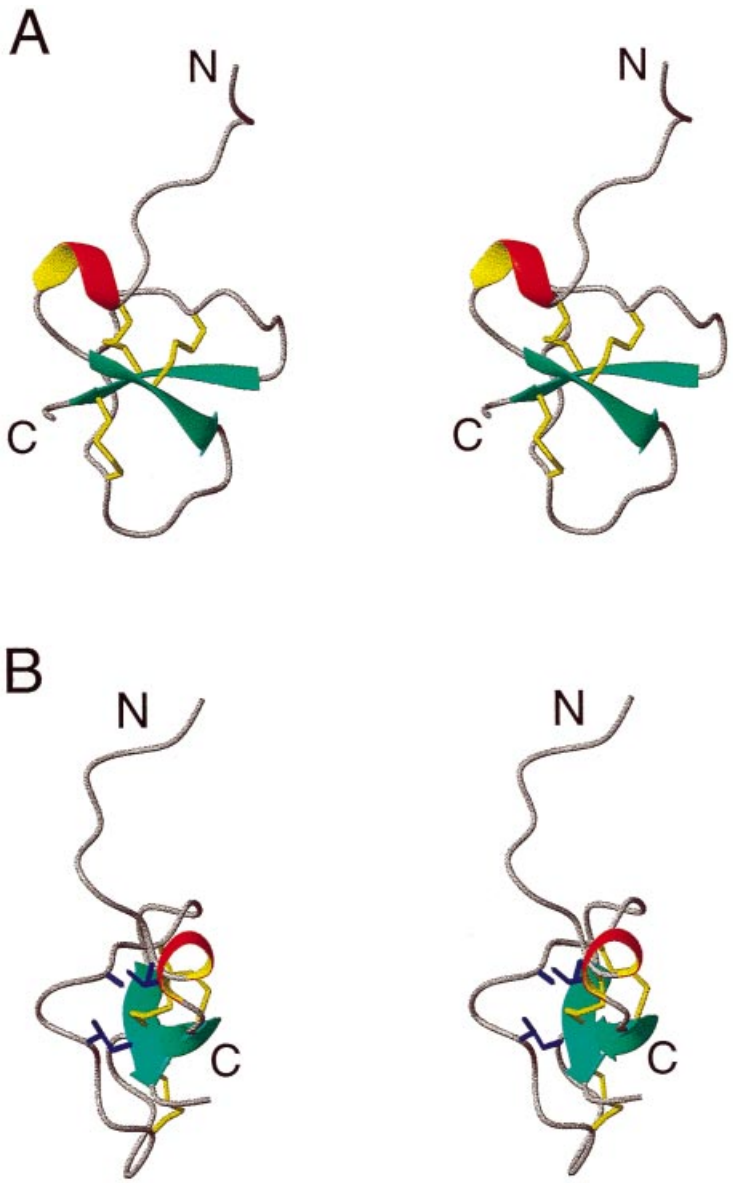

Figure 4 Schematic diagram of DLP-1 structure

(**A**) Stereo view of the schematic drawing of DLP-1 showing the locations of the disulphide bonds (yellow), β-strands (green) and 3_{10} helix (red and yellow). (**B**) Stereo view of the schematic drawing of DLP-1 showing the hydrophobic core. (**B**) is similar to (**A**) except the molecule has been rotated $\approx 90°$ about the 'virtual' vertical axis. These Figures were drawn using the program MOLMOL [45].

PROCHECK analysis [32] of the 20 structures revealed that ~ 85–90% of the non-Gly and non-Pro residues lay in the most favoured and additionally allowed regions of the Ramachandran plot. About 10–15 % of these residues resided in the 'generously allowed' region. Occasionally, some residues in the less defined region of the structure, such as Arg-5 and Arg-7, lay outside the 'sterically allowed' portion of the plot.

Description of DLP-1 structure

Analysis of the ensemble of DLP-1 structures using PROCHECK and PROMOTIF [33] revealed that residues 15–18 and 37–40 formed an anti-parallel β-sheet whereas residues 10–12 formed a short 3_{10} helix (see Figure 4A). The Arg-5–Pro-6 peptide bond is *trans*, as indicated by a strong NOE cross-peak between Hα of Arg-5 and Hδ protons of Pro-6. There is a possibility that residues 7–8 together with residues 30–31 form a short parallel β-sheet, as found in five out of the 20 structures. Residues 13–14 connect the short 3_{10} helix to the anti-parallel β-sheet defined by residues 15–18 and 37–40. There is a bend at residue 13 in this connecting segment, making the helical axis of residues 10-12 approximately parallel to the β-strand defined by residues 15–18.

The presence of the two anti-parallel β-strands defined by residues 15–18 and 37–40 is supported strongly by the presence of large positive deviations of their Hα chemical shifts from random-coil positions and by the results of hydrogen–deuterium-exchange experiments. The following hydrogen bonds between the two β-strands were identified: Val-15–Cys-40, Arg-17–Lys-38, Lys-38–Arg-17 and Cys-40–Val-15. The two anti-parallel β-strands are twisted and connected by a large loop encompassing

residues 19–36, which contains a series of turns. Regions defined by residues 18–21, 21–24, 27–30, 32–35 and 34–37 form type-IV β-turns. The large loop defined by residues 19–36 surrounds the two strands on one side and passes near the second β-strand (residues 37–40) at an angle of almost 90 °. During the early stages of the structure calculations, residues 26–31 consistently formed a large β-bulge surrounding the anti-parallel β-sheets. This tendency to form a β-bulge is further supported by the Hα chemical shifts for Arg-25, Phe-26, Ile-27 and Ala-30, which were at least 0.05 ppm higher than those in random-coil conformations. If this β-bulge were indeed present, then a hairpin loop on residues 33–36 would be created as result of this structural fold. This configuration defined by the β-bulge, hairpin loop and anti-parallel β-sheets is very similar to that found in the β-defensins and *Stichodactyla helianthus* neurotoxin I (ShI), as discussed below. Lastly, the C-terminus of DLP-1 (residues 40–42) forms an inverse γ-turn. It was not clear whether the HN of Lys-42 was hydrogen-bonded to the C = O of Cys-40, due to peak overlap in the spectrum obtained in the hydrogen–deuterium-exchange experiment.

The final proposed DLP-1 structure incorporates a well-defined hydrophobic region comprising residues Cys-9, Ile-12, Ile-27, Phe-28, Leu-29, Ala-30 and Cys-39; the central core consists of the side chains of Ile-12, Ile-27 and Ala-30 (see Figure 4B). Phe-28 and Leu-29, which are situated on the outskirts of the core, have their side chains oriented away from this region and are therefore exposed to solvent. Note that although the amide-proton signals of Glu-26 and Phe-28 were broad, indicating possible intermediate exchange between conformers, the part of the molecule containing these residues was reasonably well-defined in the calculated structures, as shown in Figure 3.

The conformations of the Cys-9–Cys-39 and Cys-16–Cys-32 disulphide bridges in DLP-1 were well-defined, whereas that of Cys-24–Cys-40 were poorly defined. The lack of definition for the Cys-24–Cys-40 bridge results from the absence of key NOE cross-peaks due to peak overlap. Nonetheless, the Cys-24–Cys-40 disulphide bond was found to be left-handed in 17 out of 20 structures. The Cys-9–Cys-39 linkage was right-handed in all 20 structures, with a χ_{ss} value of 68 ± 6 °, whereas the Cys-16–Cys-32 disulphide bond was left-handed in 18 out of 20 structures, with a χ_{ss} value of -152 ± 8 °.

Comparison with β-defensin-12 and ShI structures

The co-ordinates of the 'best' DLP-1 structure were compared with those of all other structures in the Brookhaven Protein Data Bank using the DALI search algorithm [34]. This database search revealed that the DLP-1 tertiary structure had significant similarities with that of bovine β-defensin-12 [35], in accordance with the weak sequence similarity presented above. DLP-1 also had some structural similarity with ShI, a 48-residue sodium-channel neurotoxin from the sea anemone *Stichodactyla helianthus* [36,37]. The DALI search revealed that 32 of the residues in DLP-1 were topologically equivalent to those in β-defensin-12 and that 11 of these amino acid residues were identical, whereas 28 of the DLP-1 residues were topologically equivalent to those in ShI, with only five of these residues being identical.

Similarity of the overall fold with β-defensin-12

Figure 5(A) shows ribbon representations of DLP-1 and β-defensin-12 superimposed over the 32 topologically equivalent residues found by the DALI algorithm. It is clear from this comparison that the overall folds of the two peptides are very similar except for the N-terminal region (residues 1–7 in DLP-1 and 1–3 in β-defensin-12), which is disordered in both molecules. All cysteine residues found to be topologically equivalent by the DALI algorithm were disulphide-bonded in an identical fashion in each molecule. The anti-parallel β-strands in DLP-1 (15–18, 37–40) correspond closely with those in β-defensin-12 (10–13, 32–36), although one of the strands in the latter is longer by one residue. Part of the large loop in DLP-1, defined by residues 24–27 and 30–36, corresponds to the region in β-defensin-12 defined by residues 21–31, which contains a β-strand and a β-bulge. In the DLP-1 structure, a short β-strand (residues 30–31) was found in five out of 20 structures; however, as mentioned before, the segment defined by residues 26–31 in DLP-1 has a tendency to form a β-strand with a β-bulge. The unique bend in the β-hairpin loop at residues 28–31 in the β-defensin-12 molecule, which has been evocatively likened to 'the hood of an erect cobra' [38], is not as evident in DLP-1.

Differences in fine details

Although the tertiary fold of DLP-1 is very similar to that of β-defensin-12, there are some significant differences in the fine details of the structures, which suggests that the two molecules might have different biological functions. One such feature is the overall shape of the two molecules. The β-defensin-12 structure is characterized by two faces that are basically flat when only the backbone atoms are viewed. These two faces are parallel to the β-sheets, with an axis of rotational symmetry (perpendicular to the two faces) that may be considered to pass through the three anti-parallel β-strands. The side closest the first β-strand (10–13) contains hydrophobic residues, whereas the opposite side, nearest the β-sheet with a β-bulge (22–27), contains numerous cationic residues. The division between the hydrophobic and cationic residues in β-defensin-12, and the overall shape of the molecule, are illustrated in Figure 6(A). It is believed that this cationic/hydrophobic polarity of the molecule, which has also been observed on related molecules such as human neutrophil peptide (HNP)-1 and HNP-3, is essential for its anti-microbial activity [35].

The DLP-1 molecule, in comparison with β-defensin-12, is not flat due to the presence of an extended bulge formed by residues 28–30, and its longer disordered N-terminus. Furthermore, there are significant differences in the location of cationic, anionic and hydrophobic residues between the two peptides. Figure 6(B) shows a ribbon representation of DLP-1 with the hydrophobic and cationic residues highlighted, as in Figure 6(A). The DLP-1 molecule has 10 positively charged residues, four more than in β-defensin-12. These cationic residues are concentrated in three regions of the DLP-1 molecule; the positively charged ones, near the N-terminus of DLP-1, are located in a similar position to the cationic 'patch' on β-defensin-12, but the positions of the other two positively charged regions are different. Another obvious difference is that, whereas β-defensin-12 has no anionic residues, DLP-1 has six negatively charged residues. In contrast to the cationic residues in DLP-1, these basic residues do not form a cluster. Lastly, the face on DLP-1, corresponding to the hydrophobic region of β-defensin-12, does not incorporate a large number of hydrophobic residues.

Comparison with ShI

Figure 5(B) shows the backbone structures of DLP-1 and ShI aligned over the topologically equivalent residues, as determined by the DALI search. Although the sequence similarity between the two molecules is weak, the overall fold of the two molecules is similar because the two anti-parallel β-strands and part of the

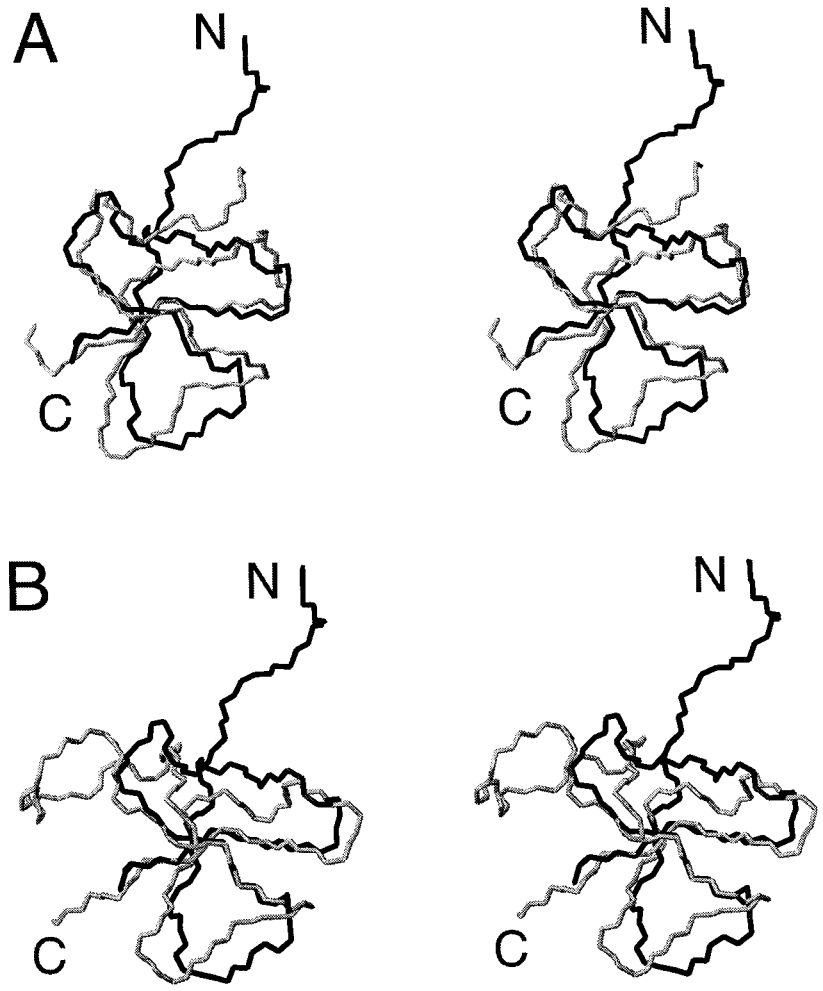

Figure 5 Comparison of the tertiary structures of DLP-1, β-defensin-12 and ShI

(**A**) Stereo view of DLP-1 and β-defensin-12 structures superimposed over the topologically equivalent N, C and Cα atoms of the backbone of residues of 8–23, 24–27 and 30–41 of DLP-1 and 4–19, 21–24 and 25–36 of β-defensin-12. DLP-1 and β-defensin-12 residues are shown in black and grey, respectively. (**B**) Stereo view of DLP-1 and ShI structures superimposed over the topologically equivalent N, C, and Cα atoms of the backbone of residues of 11–23, 24–28 and 32–41 of DLP-1 and 16–28, 30–34 and 36–45 of ShI. DLP-1 and ShI residues are shown in black and grey, respectively.

large connecting loop in DLP-1 coincide with the three major strands of the anti-parallel β-sheets in ShI. This distinct general fold, which is equivalent to that in β-defensin-12, is characterized by a C-terminal β-strand sandwiched between either two anti-parallel strands, as in the case for ShI and β-defensin-12, or an anti-parallel β-strand and a loop, as in the case for DLP-1. It is likely that the identical disulphide linkages in the three molecules play an important role in achieving the similar compact configurations.

Besides similarity in the overall fold, another significant similarity between DLP-1 and ShI is that the region near their C-terminus is highly cationic. In ShI, residues Arg-45, Lys-46, Lys-47 and Lys-48 define this strongly positively charged region, whereas in DLP-1 residues Arg-41, Lys-42 and Arg-25 form this region.

Perhaps the most significant difference in the tertiary fold of DLP-1 and ShI is that the large flexible loop near the N-terminus in ShI has no equivalent in DLP-1. This flexible loop contains three consecutive anionic residues, Asp-6, Asp-7 and Glu-8, which are known to be important in the activity of this sea anemone toxin. In addition, the locations of the hydrophobic region in the two molecules are entirely different. In ShI, the region around the tight turn at residues 38–41, which connects the second and third major β-strands, and the surrounding region, are highly hydrophobic, whereas in DLP-1 the hydrophobic region is situated on the extended part of the large loop corresponding to the second β-strand of ShI.

The framework similarities with ShI, anthopleurin-A (AP-A), *Anemonia sulcata* toxin (ATX)-II and myotoxins

In addition to the DALI search, the DLP molecular framework was compared with other known peptidic frameworks. In this comparison the emphasis was placed on the disulphide linkages rather than the three-dimensional fold. The results showed that DLP-1, which is characterized by a 1–5, 2–4 and 3–6 disulphide connectivity and $CX_6CX_7CX_7CX_6CCX_2$ pattern, had some similarities with the sea anemone toxins ShI, ATX-II and AP-A, ($CXCX_{20-22}CX_6CX_{8-9}CCX$) [39] and rattlesnake myotoxins ($X_3CX_6CX_6CX_{11}CX_5CCX_{4-7}$) [40,41]. As mentioned earlier, the DALI search had indicated that ShI, which has a similar tertiary fold to that of ATX-II and AP-A, is structurally similar to DLP-

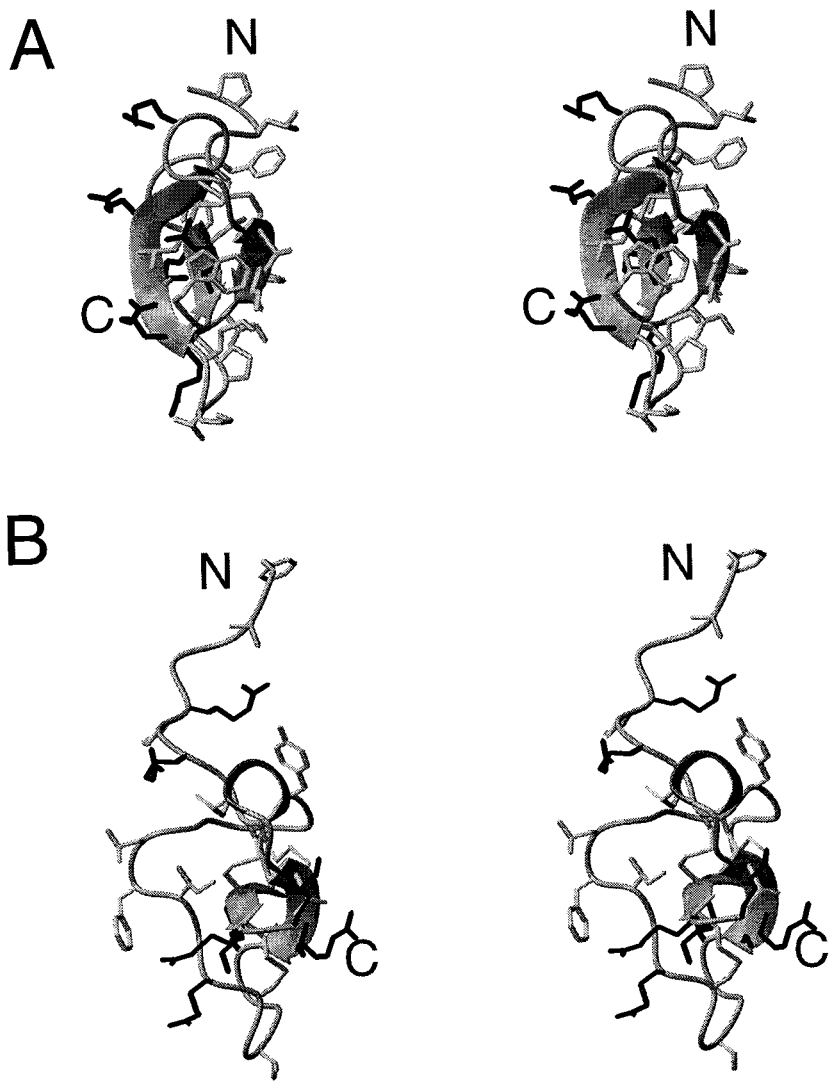

Figure 6 Detailed comparison of the structures of DLP-1 and β-defensin-12

Stereo view of schematic drawing of DLP-1 (**A**) and β-defensin-12 (**B**) showing the overall shape of the molecule and the locations of selected residues. Side-chain heavy atoms of hydrophobic residues are shown in light grey while those of cationic residues are shown in black.

1. The solution structures of rattlesnake myotoxins have not been solved yet due to isomerization problems, which were probably caused by *cis–trans* isomerism of a proline residue [42].

Biological activities

The whole and fractionated components of the platypus venom were tested on rat vas deferens in order to evaluate the relaxant activity. Whereas the whole venom, and C-type natriuretic peptide, caused strong relaxation of the rat vas deferens, the non-protein components that elute early during RP-HPLC separation caused contraction. None of the DLP peptides had any effect on the vas deferens. Subsequent tests on rat dorsal-root-ganglion sodium-channel currents, using various concentrations of DLP-1, failed to show any alteration in the amplitude, kinetics or voltage-dependence of activation of sodium currents, suggesting that its function is different from that of ShI.

The anti-microbial activity of DLP-1 and the whole platypus venom were evaluated by radial diffusion assay using *E. coli* (Gram negative) and *B. subtilis* (Gram positive) as test organisms. Neither DLP-1 nor whole venom produced any growth-free zone on the plate, indicating that they were not active against the two bacteria tested and that the biological function of DLP is different from defensins. Efforts are underway to determine whether DLP peptides exhibit any myotoxic activity.

In summary, we present three DLPs isolated from platypus venom. The tertiary structure of DLP-1 was solved using NMR spectroscopy and found to have strong similarities with the tertiary fold of β-defensin-12. However, unlike β-defensin-12, DLP-1 showed no anti-microbial activity in any of the systems tested. Detailed comparison of the structures of DLP-1 and β-defensin-12 shows that although their overall fold is similar, there are significant differences in the location of the key side-chains, suggesting that their biological functions would be likely to be different. The overall fold of DLP-1 is also similar to that of ShI, a sea anemone toxin, although their sequence similarity is very weak. However, we showed that DLP-1 had no effect on sodium-channel currents of rat dorsal-root ganglion, indicating

that its molecular target is probably different from that of ShI. Besides having similar folds, DLP-1, β-defensin-12 and ShI have identical disulphide linkages of 1–5, 2–4 and 3–6. Since the function of these three peptides appears to be unrelated (antimicrobial for β-defensin-12, capture of prey for ShI), it is tempting to speculate that the structural scaffold shared by these three peptides has been utilized widely in Nature for simple and yet effective presentation of active side-chains [35,43]. More tests are clearly needed to determine the actual role of DLP molecules in the platypus venom.

This work was supported by the Australian Research Council as a grant to P.W.K. We thank Associate Professor Mac Christie and Dr. Mark Connor for assistance in setting-up the vas deferens assays, Dr. Bill Bubb for help with the NMR spectrometer, Ms. Liesl Strachan for contributions to the electrophysiology experiments, Dr J. Wilne for early assistance with synthesizing DLP-1, and Mr. Bill Lowe for expert technical assistance.

REFERENCES

1 Calaby, J. H. (1968) in Venomous Animals and Their Venoms, vol. 1 (Bucherl, W., Buckley, E. E. and Deulofeu, V., eds.), pp. 15–29, Academic Press, New York
2 Fleay, D. (1980) Paradoxical Platypus, Jacaranda Press, Brisbane
3 Sutherland S. K. (1983) Australian Animal Toxins: the Creatures, their Toxins and Care of the Poisoned Patient, Oxford University Press, Melbourne
4 Grant, T. (1989) The Platypus, a Unique Mammal, New South Wales University Press, Kensington, NSW
5 Burell, H. (1927) The Platypus, Angus & Robertson, Sydney
6 Edstrom, A. (1992) Venomous and Poisonous Animals, Krieger Publishing Company, Florida
7 Fenner, P. J., Williamson, J. A. and Myers, D. (1992) Med. J. Aust. **157**, 829–832
8 Martin, C. J. and Tidswell, F. (1895) Proc. Linn. Soc. NSW **9**, 471–500
9 Kellaway, C. H. and LeMessurier, D. H. (1935) Aust. J. Exp. Biol. Med. Sci. **13**, 205–221
10 De Plater, G., Martin, R. L. and Milburn, P. J. (1995) Toxicon **33**, 157–169
11 De Plater, G., Martin, R. L. and Milburn, P. J. (1998) Toxicon **36**, 847–857
12 Craik, D., Munro, S., Nielsen, K., Shehan, P., Tregar, G. and Wade, J. (1991) Eur. J. Biochem. **201**, 183–190
13 Inooka, H., Kikuchi, T., Endo, S., Ishibashi, Y., Wakimasu, M. and Mizuta, E. (1990) Eur. J. Biochem. **193**, 127–134
14 Weber, J., Rösch, P., Adermann, K., Forssmann, W. G. and Wokaun, A. (1994) Biochim. Biophys. Acta **1207**, 231–235
15 Selsted, M. E., Tang, Y. Q., Morris, W. L., McGuire, P. A., Novotny, M. J., Smith, W., Henschen, A. H. and Cullor, J. S. (1993) J. Biol. Chem. **228**, 6641–6648

Received 1 March 1999/21 April 1999; accepted 11 May 1999

16 Kent, S. B. H., Hood, L. E., Beilan, H., Meister, S. and Geiser, T. (1984) in Peptides 1984: Proceedings of the 18th European Peptide Symposium (Ragnarsson, U., ed.), pp. 185–188, Almqvist and Wicksell, Stockholm
17 Kent, S. B. H., Alewood, D., Alewood, P. F., Baca, M., Jones, A. and Schnolzer, M. (1992) in Innovations and Perspectives in Solid Phase Synthesis (Epton, R., ed.), pp. 1–22, Intercept Limited, Andover
18 Nicholson, G. M., Willow, M., Howden, M. E. H. and Narahashi, T. (1994) Pflügers Arch. **428**, 400–409
19 Marion, D. and Wüthrich, K. (1983) Biochem. Biophys. Res. Commun. **113**, 967–974
20 Rance, M., Sørensen, O. W., Bodenhausen, G., Wagner, G., Ernst, R. R. and Wüthrich, K. (1983) Biochem. Biophys. Res. Commun. **117**, 479–465
21 Derome, A. E. and Williamson, M. P. (1990) J. Magn. Reson. **88**, 177–185
22 Bax, A. and Davis, D. G. (1985) J. Magn. Reson. **65**, 355–360
23 Kumar, A., Ernst, R. R. and Wüthrich, K. (1980) Biochem. Biophys. Res. Commun. **95**, 1–6
24 Piotto, M., Saudek, V. and Sklenár, V. (1992) J. Biomol. NMR **2**, 661–665
25 Bartels, C., Xia, T., Billeter, M., Güntert, P. and Wüthrich, K. (1995) J. Biomol. NMR **5**, 1–10
26 Szyperski, I., Güntert, P., Otting, G. and Wüthrich, K. (1992) J. Magn. Reson. **99**, 552–560
27 Ludvigsen, S. and Poulsen, F. M. (1992) J. Biomol. NMR **2**, 227–233
28 Güntert, P., Mumenthaler, C. and Wüthrich, K. (1997) J. Mol. Biol. **273**, 283–298
29 Brünger, A. T. (1992) X-PLOR Version 3.1. A System for X-Ray Crystallography and NMR, Yale University, New Haven
30 Wüthrich, K. (1986) NMR of Proteins and Nucleic Acids, John Wiley, New York
31 Hyberts, S. G., Goldberg, M. S., Havel, T. F. and Wagner, G. (1992) Protein. Sci. **1**, 736–751
32 Laskowski, R. A., MacArthur, M. W., Moss, D. S. and Thorton, J. M. (1993) J. Appl. Crystallogr. **26**, 283–292
33 Hutchinson, E. G. and Thorton, J. M. (1996) Protein. Sci. **5**, 212–220
34 Holm, L. and Sander, C. (1993) J. Mol. Biol. **233**, 123–138
35 Zimmermann, G. R., Legault, P., Selsted, M. E. and Pardi, A. (1995) Biochemistry **34**, 13663–13671
36 Fogh, R. H., Kem, W. R. and Norton, R. S. (1990) J. Biol. Chem. **265**, 13016–13028
37 Wilcox, G. R., Fogh, R. H. and Norton, R. S. (1993) J. Biol. Chem. **267**, 24707–24719
38 Sibanda, B. L. and Thornton, J. M. (1985) Nature (London) **216**, 170–174
39 Gould, A. L., Mabbutt, B. C., Llewellyn, L. E., Goss, N. H. and Norton, R. S. (1992) Eur. J. Biochem. **206**, 641–651
40 Fox, J. W., Elzinga, M. and Tu, A. T. (1979) Biochemistry **18**, 678–684
41 Mebs, D. and Ownby, C. L. (1990) Pharmac. Ther. **48**, 228–236
42 O'Keefe, M. P., Nedelkov, D., Bieber, A. L. and Nieman, R. A. (1996) Toxicon **34**, 417–434
43 Norton, R. S. and Pallaghy, P. K. (1998) Toxicon **36**, 1573–1583
44 Barton, G. J. (1993) Protein. Eng. **6**, 37–40
45 Koradi, R., Billeter, M. and Wüthrich, K. (1996) J. Mol. Graph. **14**, 51–55